
Certified defences hurt generalisation

Anonymous Author(s)

Affiliation

Address

email

Abstract

1 In recent years, much work has been devoted to designing certified defences for
2 neural networks, i.e., methods for learning neural networks that are provably robust
3 to certain adversarial perturbations. Due to the non-convexity of the problem, dom-
4 inant approaches in this area rely on convex approximations, which are inherently
5 loose. In this paper, we question the effectiveness of such approaches for realistic
6 computer vision tasks. First, we provide extensive empirical evidence to show that
7 certified defences suffer not only worse accuracy but also worse robustness and
8 fairness than empirical defences. We hypothesise that the reason for why certified
9 defences suffer in generalisation is (i) the large number of relaxed non-convex
10 constraints and (ii) the strong alignment between the adversarial perturbations and
11 the "signal" direction. We provide a combination of theoretical and experimental
12 evidence to support these hypotheses.

13 1 Introduction

14 Several works have shown the existence of adversarial examples: imperceptible perturbations to the
15 input can fool state-of-the-art classifiers [2, 22]. Consequently, robustness to adversarial examples
16 has become a crucial design goal for machine learning models. In real-world scenarios, robustness
17 against many different types of input perturbations may be desired depending on the domain of
18 application. Therefore, to build robust models, we must first define a threat model for the adversary.
19 In this paper, we consider the well-studied ℓ_p -ball threat model, where $\mathcal{B}_\epsilon := \{\delta : \|\delta\|_p \leq \epsilon\}$
20 represents the set of allowed perturbations for some ℓ_p -ball with radius ϵ centred around the origin.
21

22 Once a threat model is defined, we can formalise the problem of building models that are
23 robust to adversarial examples. For any distribution \mathcal{D} , neural network model $f_\theta : \mathbb{R}^d \rightarrow \mathbb{R}^k$
24 parameterised by the weights $\theta \in \mathbb{R}^p$, and loss function L , our goal is to solve the following robust
25 optimisation problem:

$$\min_{\theta} \mathbf{R}_\epsilon(\theta) := \mathbb{E}_{(x,y) \sim \mathcal{D}} \left[\max_{\delta \in \mathcal{B}_\epsilon} L(f_\theta(x + \delta), y) \right] \quad (1)$$

26 We call $\mathbf{R}_\epsilon(\theta)$ the robust error when L is the 0-1 loss function. In practice, as the distribution \mathcal{D} is
27 unknown, we minimise the empirical robust error on a finite dataset D sampled from \mathcal{D} . Further,
28 in the case of neural networks, the inner-maximisation is a non-convex optimisation problem and
29 prohibitively hard to solve from a computational perspective [12, 24]. Instead, two efficient techniques
30 are widely used to overcome the computational barrier: *empirical* defences that provide a lower
31 bound on the solution and *certified* defences that provide an upper bound.

32 Among empirical defences, Adversarial Training (AT) [11, 16] is one of the few that has stood the
33 test of time. AT minimises the worst-case empirical loss in Equation (1) by approximately solving
34 the inner-maximisation problem with first-order gradient-based optimisation methods. However,
35 despite its simplicity and computational efficiency, owing to its heuristic nature, AT is incapable of

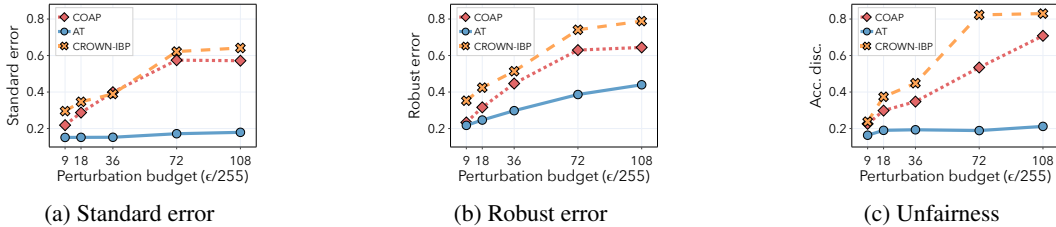


Figure 1: Results for ℓ_2 -adversaries on the CIFAR-10 dataset. We compare ResNet architectures trained using state-of-the-art certified defenses CROWN-IBP [31, 28] and COAP [26, 25] against the most popular empirical defense to date AT [16, 11]. In Figures 1a, 1b and 2g we plot respectively standard error, robust error and accuracy discrepancy as the perturbation budget increases. See Appendix D.3 for complete experimental details.

36 guaranteeing that no adversarial examples exist. In many safety critical domains, such guarantees are
 37 of immense importance.

38 To address this limitation, recently, there has been significant interests in designing certified defences,
 39 i.e., methods for learning neural networks that are *provably* robust to norm-bounded perturbations
 40 on the training data. Many recent works [25, 18, 7, 31] have proposed to solve a convex relaxation
 41 of the inner-maximisation problem by relaxing the non-convex ReLU constraint sets with convex
 42 ones. Despite all of these progresses, certified defences based on convex relaxations suffer from an
 43 inherent flaw: the upper bound they provide on the robust error is far from being tight due to the
 44 looseness of the convex relaxation [20]. In this paper, we argue that the fundamental looseness of
 45 convex relaxations hinders the practical effectiveness of current certified defences. In particular, as
 46 shown in Figure 1, certified defences suffer significantly worse accuracy, robustness, and fairness on
 47 the test data compared to adversarial training. Our contributions are as follows:

- 48 • In Section 2, we show that current certified defences hurt accuracy, robustness, and fairness across
 49 a range of ℓ_2 -ball perturbations on real-world vision datasets like MNIST and CIFAR-10.
- 50 • In Section 3, we provide experimental evidence that certified defences hurt generalisation because
 51 of (i) the large number of relaxed non-convex constraints and (ii) strong alignment between the
 52 adversarial perturbations and the signal direction.

53 2 Certified defences hurt generalisation on real-world data

54 In this section, we show that certified defences hurt standard error, robust error, and fairness on two
 55 common computer vision datasets: MNIST [15] and CIFAR-10 [14]. Among certified defences,
 56 we consider the convex outer adversarial polytope (COAP) [26, 25], which achieves state-of-the-art
 57 certified robustness under ℓ_2 -ball perturbations. Additionally, we consider CROWN-IBP [30, 28],
 58 which uses the tight convex relaxation CROWN [30] and achieves state-of-the-art certified robustness
 59 under ℓ_∞ -ball perturbations. Among empirical defences, we consider adversarial training (AT) [16,
 60 11], which is one of the most popular and effective defences to date.

61 **Models and robust evaluation** We consider the ℓ_2 -ball perturbations threat model. To reliably
 62 evaluate the robust error, we use the strongest version of AutoAttack (AA+) [5]. For CIFAR-10, we
 63 train a residual network (ResNet) and for MNIST we train a large convolutional neural network (CNN).
 64 Both architectures were introduced in Wong et al. [26] as standard benchmarks for certified defences.

65 **Certified defences hurt standard and robust error** Several studies have shown that adversarial
 66 training may lead to an increase in standard error when compared with standard training [19, 23, 29].
 67 We observe the same phenomenon to a much higher degree in certified defences. Our experimen-
 68 tal results show that certified defences not only suffer worse standard error but also worse robust
 69 error than adversarial training. First, we observe on both MNIST and CIFAR-10 in Figures 2a
 70 and 2c, respectively, that for increasing perturbation budget, the standard error gap between certi-
 71 fied (CROWN-IBP, COAP) and empirical defences (AT) increases. Secondly, we observe that the
 72 robust error gap increases with increasing perturbation budget for both MNIST and CIFAR-10 in
 73 Figures 2b and 2d, respectively.

74 **Certified defences hurt fairness** Previously, we showed that certified defences hurt both standard
 75 and robust generalisation. Taking it one step further, we show that certified defences (CROWN-IBP,
 76 COAP) suffer significantly worse fairness than empirical defences (AT). Let $\mathbf{R}(\theta)$ be the standard

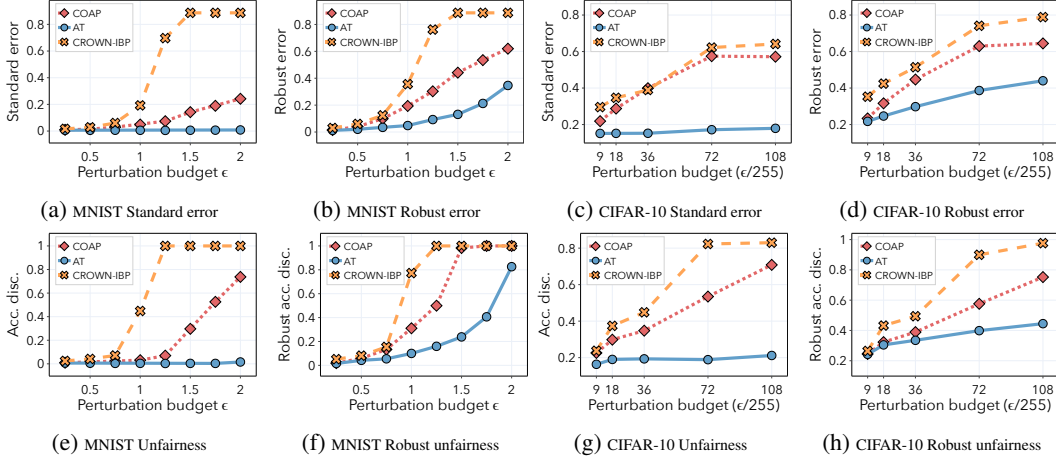


Figure 2: Results for ℓ_2 -adversaries on MNIST and CIFAR-10 datasets. In Figures 2a, 2b, 2e and 2f we plot respectively the standard error, robust error, accuracy discrepancy and robust accuracy discrepancy for a CNN trained on MNIST, as the perturbation budget ϵ increases. In Figures 2c, 2d, 2g and 2h we plot respectively the standard error, robust error, accuracy discrepancy and robust accuracy discrepancy, for a ResNet trained on CIFAR-10, as the perturbation budget ϵ increases.

77 error of the classifier f_θ and $\mathbf{R}^k(\theta)$ the standard error conditioned on the class label k . We measure
78 the degree of unfairness as follows: $(\max_k \mathbf{R}^k(\theta) - \mathbf{R}(\theta))(1 - \mathbf{R}(\theta))^{-1}$. Using the terminology in
79 Sanyal et al. [21], we refer to this metric as *accuracy discrepancy*. Similarly, we also consider the
80 discrepancy in robust accuracy, as it was observed in Xu et al. [27] that adversarial defences may
81 induce a large discrepancy of robustness among different classes. We refer to this metric as *robust*
82 *accuracy discrepancy* where we replace the standard error with the robust error.

83 We present our experimental results comparing the fairness of certified and empirical defences. For
84 MNIST, we observe in Figure 2e and 2f that COAP and CROWN-IBP have a significant discrepancy
85 for both standard and robust accuracy. For large perturbations, these methods obtain 100% discrepan-
86 cy, indicating that their accuracy on the worst class can be as low as 0%. By contrast, AT preserves
87 fairness for both standard and robust accuracy much better. In particular, the discrepancy for standard
88 accuracy is always less than 2% for all perturbation budgets considered. Similarly, for CIFAR-10
89 AT maintains a constant accuracy discrepancy around 20% for all perturbation budgets considered,
90 whereas for certified defences it steadily increases with the perturbation budget, reaching above 80%.
91 Additionally, for robust accuracy, we observe a discrepancy gap of 35% between the best certified
92 and empirical defences for the largest perturbation budget considered.

93 3 Developing intuition on synthetic datasets

94 In this section, we hypothesise that certified defences hurt robust and standard generalisation because
95 of (i) the large number of relaxed non-convex constraints and (ii) strong alignment between the
96 adversarial perturbations and the signal direction. We investigate these hypotheses on more controlled
97 settings. Specifically, we consider two synthetic data distributions: a linearly separable distribution as
98 in Clarysse et al. [4], which is similar to the one in in Nagarajan and Kolter [17], Tsipras et al. [23],
99 and the concentric spheres distribution studied in Gilmer et al. [10], Nagarajan and Kolter [17].

100 **Data and threat models** Similarly to the previous section, we focus on ℓ_2 -ball perturbations of
101 size ϵ . As for distributions, we consider the linearly separable distribution where first, the label
102 $y \in \{+1, -1\}$ is drawn with equal probability. Then, for some $\gamma > 0$, the covariate vector is created
103 as $x = [\gamma \text{sgn}(y); \tilde{x}]$, where $\tilde{x} \in \mathbb{R}^{d-1}$ is a random vector drawn from a standard normal distribution
104 $\tilde{x} \sim \mathcal{N}(0, \sigma^2 I_{d-1})$ and $[\cdot; \cdot]$ represents concatenation. We sample the concentric spheres dataset as
105 follows; for $0 < R_1 < R_{-1}$, we first draw a binary label $y \in \{+1, -1\}$ with equal probability and
106 then the covariate vector $x \in \mathbb{R}^d$ is distributed uniformly on the sphere of radius R_y . Observe that
107 achieving a low test error on the concentric spheres distribution requires a non-linear classifier.

108 In Figure 3e and 3f, we plot the robust error of standard training (ST), adversarial training (AT),
109 and certified training (COAP) on the linear and concentric spheres distributions respectively. We

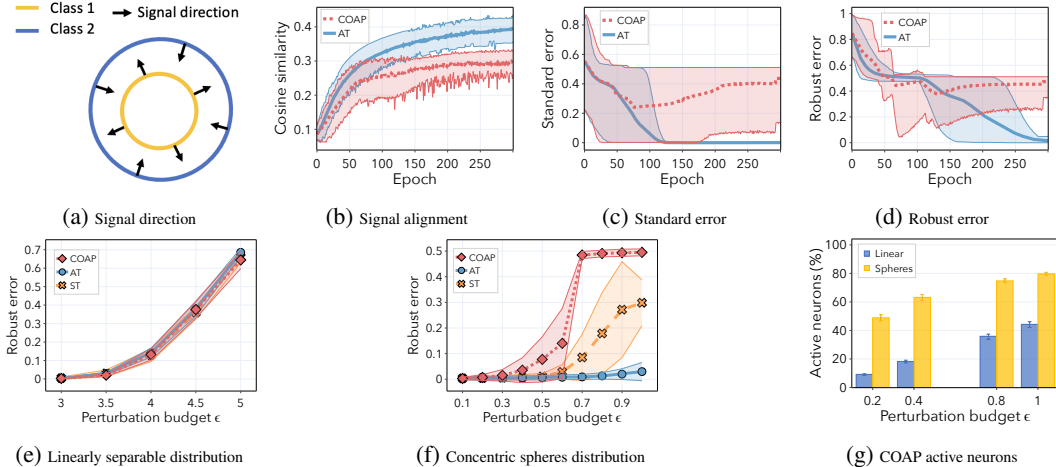


Figure 3: We report mean and standard deviation over 15 seeds. In Figures 3e and 3f we plot the robust error for standard training (ST), adversarial training (AT) and convex outer adversarial polytope (COAP), when training on the linearly separable and concentric spheres distributions respectively. In Figure 3g, we plot the percentage of neurons in the activation set for the linearly separable and concentric spheres distribution respectively. In Figure 3a we plot a 2-D visualisation of the concentric spheres dataset, the black arrow illustrates the signal direction. In Figure 3b we plot the cosine similarity between ℓ_2 -ball perturbations on the training data (average) and the signal directed vector. In Figure 3c and 3d we plot standard and robust error for adversarial training (AT) and convex outer adversarial polytope (COAP).

110 see that in contrast to the linear setting, COAP has a much higher robust error on the concentric
 111 spheres distribution than AT and ST, where the gap increases for increasing perturbation budget
 112 ϵ . The intuition for why this happens is two-fold: first of all COAP relaxes the non-convex ReLU
 113 constraints for all neurons that activate within the perturbation set, i.e., there exists $\delta \in \mathcal{B}_\epsilon$ for which
 114 the input to the neuron equals 0. Hence, the larger the percentage of relaxed neurons, the worse the
 115 approximation. This is formally captured by Theorem A.1 in Appendix A. Secondly, the ℓ_2 -ball
 116 perturbations are significantly aligned with the signal direction, meaning that they effectively reduce
 117 the information about the label in the data. Applying an approximation in this direction yields poor
 118 generalisation. We prove this in Theorem B.1 in Appendix B for the linearly separable distribution.

119 **COAP relaxes many constraints on the concentric spheres** In Figure 3g we empirically show
 120 that COAP convexly approximates a large number of constraints when training on the concentric
 121 spheres distribution. We plot the percentage of active neurons on the concentric spheres and linear
 122 distributions against increasing perturbation budgets: the percentage is much higher for the concentric
 123 spheres than for the linearly separable distribution and increases with perturbation budget ϵ . Indeed,
 124 the complex spherical decision boundary requires much more active neurons compared to the linear
 125 decision boundary which only needs 1 active neuron.

126 **ℓ_2 -ball perturbations align with the signal direction** We empirically show that ℓ_2 -ball perturba-
 127 tions align with the signal direction on the concentric spheres distribution. Note that for a point x
 128 drawn from the concentric spheres distribution, the signal direction is given by $y \frac{x}{\|x\|_2}$ (see Figure 3a
 129 for a 2D visualization). In Figure 3b, we plot the cosine distance between the ℓ_2 -perturbations
 130 computed on the training set, and the signal direction. Comparing Figures 3b to 3d, we see that during
 131 the early stages of training, the ℓ_2 -ball perturbations are not aligned with the signal direction and the
 132 robust and standard errors for COAP are similar to AT. However, after some epochs, when the ℓ_2 -ball
 133 perturbations start to align with the signal direction, both the robust and standard error gaps between
 134 COAP and AT increase. This provides evidence that, as training progresses, ℓ_2 -ball perturbations
 135 become significantly aligned with the signal direction and the generalisation gap worsens.

136 **4 Conclusions**

137 In this paper, we show that certified defences can hurt robustness, accuracy and fairness for realistic
 138 datasets and adversarial perturbations. Further, we develop intuition on synthetic datasets for why
 139 certified defences hurt generalisation, combining both theoretical and experimental evidence. We
 140 believe that understanding the performance gap between empirical and certified defences will lead to
 141 better approaches for adversarial robustness.

References

- [1] Jimmy Ba, Murat A. Erdogdu, Taiji Suzuki, Zhichao Wang, Denny Wu, and Greg Yang. High-dimensional Asymptotics of Feature Learning: How One Gradient Step Improves the Representation, May 2022. arXiv:2205.01445 [cs, math, stat].
- [2] Battista Biggio, Iginio Corona, Davide Maiorca, Blaine Nelson, Nedim Srndic, Pavel Laskov, Giorgio Giacinto, and Fabio Roli. Evasion Attacks against Machine Learning at Test Time. In *Machine Learning and Knowledge Discovery in Databases - European Conference*, 2013.
- [3] Niladri S. Chatterji, Philip M. Long, and Peter L. Bartlett. When Does Gradient Descent with Logistic Loss Find Interpolating Two-Layer Networks? *Journal of Machine Learning Research*, (159), 2021. ISSN 1533-7928.
- [4] Jacob Clarysse, Julia Hörrmann, and Fanny Yang. Why adversarial training can hurt robust accuracy, 2022. arXiv:2203.02006.
- [5] Francesco Croce and Matthias Hein. Reliable evaluation of adversarial robustness with an ensemble of diverse parameter-free attacks. In *Proceedings of the International Conference on Machine Learning*, 2020.
- [6] Amit Daniely and Eran Malach. Learning Parities with Neural Networks. In *Advances in Neural Information Processing Systems*, 2020.
- [7] Krishnamurthy Dvijotham, Robert Stanforth, Sven Gowal, Timothy A. Mann, and Pushmeet Kohli. A Dual Approach to Scalable Verification of Deep Networks. In *Proceedings of the Conference on Uncertainty in Artificial Intelligence*, 2018.
- [8] Ecenaz Erdemir, Jeffrey Bickford, Luca Melis, and Sergül Aydıre. Adversarial Robustness with Non-uniform Perturbations. In *Advances in Neural Information Processing Systems*, 2021.
- [9] Spencer Frei, Niladri S. Chatterji, and Peter L. Bartlett. Random Feature Amplification: Feature Learning and Generalization in Neural Networks, May 2022. arXiv:2202.07626 [cs, math, stat].
- [10] Justin Gilmer, Luke Metz, Fartash Faghri, Samuel S. Schoenholz, Maithra Raghu, Martin Wattenberg, and Ian J. Goodfellow. Adversarial Spheres. *CoRR*, 2018. arXiv: 1801.02774.
- [11] Ian J. Goodfellow, Jonathon Shlens, and Christian Szegedy. Explaining and Harnessing Adversarial Examples. In *Proceedings of the International Conference on Learning Representations*, 2015.
- [12] Guy Katz, Clark W. Barrett, David L. Dill, Kyle Julian, and Mykel J. Kochenderfer. Reluplex: An Efficient SMT Solver for Verifying Deep Neural Networks. In *Proceedings of the International Conference of Computer Aided Verification*, 2017.
- [13] Diederik P. Kingma and Jimmy Ba. Adam: A Method for Stochastic Optimization. In *Proceedings of the International Conference on Learning Representations*, 2015.
- [14] Alex Krizhevsky. Learning multiple layers of features from tiny images. *citeseer*, 2009.
- [15] Yann LeCun, Léon Bottou, Yoshua Bengio, and Patrick Haffner. Gradient-based learning applied to document recognition. *Proc. IEEE*, (11), 1998.
- [16] Aleksander Madry, Aleksandar Makelov, Ludwig Schmidt, Dimitris Tsipras, and Adrian Vladu. Towards Deep Learning Models Resistant to Adversarial Attacks. In *Proceedings of the International Conference on Learning Representations*, 2018.
- [17] Vaishnavh Nagarajan and J. Zico Kolter. Uniform convergence may be unable to explain generalization in deep learning. In *Advances in Neural Information Processing Systems*, 2019.
- [18] Aditi Raghunathan, Jacob Steinhardt, and Percy Liang. Certified Defenses against Adversarial Examples. In *Proceedings of the International Conference on Learning Representations*, 2018.

- 186 [19] Aditi Raghunathan, Sang Michael Xie, Fanny Yang, John C. Duchi, and Percy Liang. Under-
187 standing and Mitigating the Tradeoff between Robustness and Accuracy. In *Proceedings of*
188 *the 37th International Conference on Machine Learning, ICML 2020, 13-18 July 2020, Virtual*
189 *Event*, volume 119 of *Proceedings of Machine Learning Research*, pages 7909–7919. PMLR,
190 2020. URL <http://proceedings.mlr.press/v119/raghunathan20a.html>.
- 191 [20] Hadi Salman, Greg Yang, Huan Zhang, Cho-Jui Hsieh, and Pengchuan Zhang. A Convex
192 Relaxation Barrier to Tight Robustness Verification of Neural Networks. In *Advances in Neural*
193 *Information Processing Systems*, 2019.
- 194 [21] Amartya Sanyal, Yaxi Hu, and Fanny Yang. How unfair is private learning? In *Proceedings of*
195 *the Conference on Uncertainty in Artificial Intelligence*, 2022.
- 196 [22] Christian Szegedy, Wojciech Zaremba, Ilya Sutskever, Joan Bruna, Dumitru Erhan, Ian J.
197 Goodfellow, and Rob Fergus. Intriguing properties of neural networks. In *Proceedings of the*
198 *International Conference on Learning Representations*, 2014.
- 199 [23] Dimitris Tsipras, Shibani Santurkar, Logan Engstrom, Alexander Turner, and Aleksander Madry.
200 Robustness May Be at Odds with Accuracy. In *Proceedings of the International Conference on*
201 *Learning Representations*, 2019.
- 202 [24] Tsui-Wei Weng, Huan Zhang, Hongge Chen, Zhao Song, Cho-Jui Hsieh, Luca Daniel, Duane S.
203 Boning, and Inderjit S. Dhillon. Towards fast computation of certified robustness for relu
204 networks. In *Proceedings of the International Conference on Machine Learning*, 2018.
- 205 [25] Eric Wong and J. Zico Kolter. Provable Defenses against Adversarial Examples via the Convex
206 Outer Adversarial Polytope. In *Proceedings of the International Conference on Machine*
207 *Learning*, 2018.
- 208 [26] Eric Wong, Frank R. Schmidt, Jan Hendrik Metzen, and J. Zico Kolter. Scaling provable
209 adversarial defenses. In *Advances in Neural Information Processing Systems*, 2018.
- 210 [27] Han Xu, Xiaorui Liu, Yaxin Li, Anil K. Jain, and Jiliang Tang. To be Robust or to be Fair:
211 Towards Fairness in Adversarial Training. In *Proceedings of the International Conference on*
212 *Machine Learning*, Proceedings of Machine Learning Research, 2021.
- 213 [28] Kaidi Xu, Zhouxing Shi, Huan Zhang, Yihan Wang, Kai-Wei Chang, Minlie Huang, Bhavya
214 Kaillkhura, Xue Lin, and Cho-Jui Hsieh. Automatic Perturbation Analysis for Scalable Certified
215 Robustness and Beyond. In *Advances in Neural Information Processing Systems*, 2020.
- 216 [29] Hongyang Zhang, Yaodong Yu, Jiantao Jiao, Eric P. Xing, Laurent El Ghaoui, and Michael I.
217 Jordan. Theoretically Principled Trade-off between Robustness and Accuracy. In Kamalika
218 Chaudhuri and Ruslan Salakhutdinov, editors, *Proceedings of the 36th International Conference*
219 *on Machine Learning, ICML 2019, 9-15 June 2019, Long Beach, California, USA*, volume 97
220 of *Proceedings of Machine Learning Research*, pages 7472–7482. PMLR, 2019. URL <http://proceedings.mlr.press/v97/zhang19p.html>.
- 222 [30] Huan Zhang, Tsui-Wei Weng, Pin-Yu Chen, Cho-Jui Hsieh, and Luca Daniel. Efficient Neural
223 Network Robustness Certification with General Activation Functions. In *Advances in Neural*
224 *Information Processing Systems*, 2018.
- 225 [31] Huan Zhang, Hongge Chen, Chaowei Xiao, Sven Gowal, Robert Stanforth, Bo Li, Duane S.
226 Boning, and Cho-Jui Hsieh. Towards Stable and Efficient Training of Verifiably Robust Neural
227 Networks. In *Proceedings of the International Conference on Learning Representations*, 2020.

228 **A COAP for signal-directed adversaries**

229 In this section, we extend COAP to signal-directed adversaries, our derivation can be seen as an
 230 extension of Wong and Kolter [25], Erdemir et al. [8]. We consider the hypothesis class to be the set
 231 of one-hidden layer neural networks $f_\theta : \mathbb{R}^d \rightarrow \mathbb{R}^2$ with parameters $\theta = \{W_1, b_1, W_2, b_2\}$:

$$x \xrightarrow{x+\delta} z_1 \xrightarrow{W_1 z_1 + b_1} \hat{z}_2 \xrightarrow{\text{ReLU}(\cdot)} z_2 \xrightarrow{W_2 z_2 + b_2} \hat{z}_3 \quad (2)$$

232 where $x \in \mathbb{R}^d$ and $z_1 \in \mathcal{B}_\epsilon(x)$. We define the adversarial polytope $\mathcal{Z}_\epsilon(x)$ as the set of all final-layer
 233 activations attainable by perturbing x with some $\tilde{x} \in \mathcal{B}_\epsilon(x)$:

$$\mathcal{Z}_\epsilon(x) = \{f_\theta(\tilde{x}) : \tilde{x} \in \mathcal{B}_\epsilon(x)\} \quad (3)$$

234 Our approach will be to construct a convex outer bound on this adversarial polytope: if no adversarial
 235 example exists in this outer approximation, then we are guaranteed that no adversarial example exists
 236 in the original polytope. We relax the ReLU activations $z = \text{ReLU}(\hat{z})$ with their convex envelopes:

$$z \geq 0, \quad z \geq \hat{z}, \quad (u - \ell)z \leq u\hat{z} - u\ell \quad (4)$$

237 where u and ℓ are respectively the pre-activations \hat{z} upper and lower bounds, for which we provide a
 238 closed form solution in Appendix A.1. We define the outer bound on the adversarial polytope we get
 239 from relaxing ReLU constraints as $\tilde{\mathcal{Z}}_\epsilon(x)$. Given a sample x with known label y , we can write the
 240 linear program formulation of the adversary’s problem for our network as follows:

$$\min_{\hat{z}_3} [\hat{z}_3]_y - [\hat{z}_3]_{\bar{y}} = c^\top \hat{z}_3 \quad \text{s.t.} \quad \hat{z}_3 \in \tilde{\mathcal{Z}}_\epsilon \quad (5)$$

241 where \bar{y} is the binary negation of y . Note that if we solve this linear program and find that the
 242 objective is positive, then we know that no input perturbation can misclassify the example. Since
 243 solving the linear program (5) for every example in the dataset is intractable, we consider the dual
 244 formulation and take a feasible solution. In Theorem A.1, we state the dual problem formulation of
 245 the linear program with ReLU relaxations (5).

246 **Theorem A.1.** *The dual of the linear program (5) can be written as*

$$\begin{aligned} \max_{\alpha} \quad & \tilde{J}_\epsilon(x, g_\theta(c, \alpha)) \\ \text{s.t.} \quad & \alpha_j \in [0, 1], \quad \forall j \end{aligned} \quad (6)$$

247 where $\tilde{J}_\epsilon(x, \nu_1, \nu_2, \nu_3)$ is equal to

$$-\sum_{i=1}^2 \nu_{i+1}^\top b_i + \sum_{j \in \mathcal{I}} \ell_j [\nu_2]_j^+ - \hat{\nu}_1^\top x - \epsilon \|\hat{\nu}_1\|_1 \quad (7)$$

248 and g_θ is a one-hidden layer neural network given by the equations

$$\begin{aligned} \nu_3 &= -c \\ \hat{\nu}_2 &= W_2^\top \nu_3 \\ [\nu_2]_j &= 0, \quad j \in \mathcal{I}^- \\ [\nu_2]_j &= [\hat{\nu}_2]_j, \quad j \in \mathcal{I}^+ \\ [\nu_2]_j &= \frac{u_j}{u_j - \ell_j} [\hat{\nu}_2]_j^+ - \alpha_j [\hat{\nu}_2]_j^-, \quad j \in \mathcal{I} \\ \hat{\nu}_1 &= W_1^\top \nu_2 \end{aligned} \quad (8)$$

249 where $\mathcal{I}^-, \mathcal{I}^+$ and \mathcal{I} denote the sets of activations in the hidden layer where ℓ and u are both negative,
 250 both positive and span zero, respectively.

251 In particular, this theorem states that we can represent the dual problem as a linear back propagation
 252 network, which provides a tractable solution for a lower bound on the primal objective. In practice,
 253 rather than solving the exact dual problem, we choose the fixed, dual feasible solution: $\alpha_j = \frac{u_j}{u_j - \ell_j}$.

254 **A.1 Computing upper and lower bounds**

255 We address here the problem of obtaining the upper and lower bounds u and ℓ for the pre-activations
 256 \hat{z} , which so far we have assumed to be known. In Proposition A.2 we give a closed form solution for
 257 ℓ and u .

258 **Proposition A.2.** Consider the neural network defined in Equation (2). Let w_1 be the first column of
 259 W_1 and x be a given example, then we have the following element-wise bound:

$$\ell \leq \hat{z}_2 \leq u \quad (9)$$

260 where

$$\ell = W_1 x + b_1 - \epsilon |w_1|, \quad u = W_1 x + b_1 + \epsilon |w_1| \quad (10)$$

261 *Proof.* Given an example x , let $\tilde{x} = x + \delta$ be the perturbed input to the network. We want to upper
 262 bound the pre-activations values \hat{z}_2 :

$$\hat{z}_2 = W_1(x + \delta) + b_1 = W_1 x + b_1 + W_1 \delta \quad (11)$$

263 In particular, we want to solve the following optimisation problem for each component of the
 264 pre-activation vector:

$$u_i = \max_{\tilde{x} \in \mathcal{B}_\epsilon(x)} [\hat{z}_2]_i = [W_1 x]_i + [b_1]_i + \max_{\tilde{x} \in \mathcal{B}_\epsilon(x)} [W_1 \delta]_i \quad (12)$$

265 where u will be the vector containing element-wise upper bounds. Note that $\delta = \beta e_1$, thus the
 266 optimisation problem can be rewritten as:

$$\max_{\tilde{x} \in \mathcal{B}_\epsilon(x)} [W_1 \delta]_i = \max_{\|\beta\|_1 \leq \epsilon} \beta \cdot [w_1]_i = \epsilon \cdot \|[w_1]_i\|_1 \quad (13)$$

267 where w_1 is the first column of W_1 . The vector of upper bounds will then be:

$$u = W_1 x + b_1 + \epsilon |w_1| \quad (14)$$

268 Along the same lines, we can derive the vector of lower bounds ℓ :

$$\ell = W_1 x + b_1 - \epsilon |w_1| \quad (15)$$

269

□

270 A.2 Proof of Theorem A.1

271 **Theorem A.1.** The dual of the linear program (5) can be written as

$$\begin{aligned} \max_{\alpha} \quad & \tilde{J}_\epsilon(x, g_\theta(c, \alpha)) \\ \text{s.t.} \quad & \alpha_j \in [0, 1], \forall j \end{aligned} \quad (6)$$

272 where $\tilde{J}_\epsilon(x, \nu_1, \nu_2, \nu_3)$ is equal to

$$-\sum_{i=1}^2 \nu_{i+1}^\top b_i + \sum_{j \in \mathcal{I}} \ell_j [\nu_2]_j^+ - \hat{\nu}_1^\top x - \epsilon \|[\hat{\nu}_1]_1 \|_1 \quad (7)$$

273 and g_θ is a one-hidden layer neural network given by the equations

$$\begin{aligned} \nu_3 &= -c \\ \hat{\nu}_2 &= W_2^\top \nu_3 \\ [\nu_2]_j &= 0, \quad j \in \mathcal{I}^- \\ [\nu_2]_j &= [\hat{\nu}_2]_j, \quad j \in \mathcal{I}^+ \\ [\nu_2]_j &= \frac{u_j}{u_j - \ell_j} [\hat{\nu}_2]_j^+ - \alpha_j [\hat{\nu}_2]_j^-, \quad j \in \mathcal{I} \\ \hat{\nu}_1 &= W_1^\top \nu_2 \end{aligned} \quad (8)$$

274 where $\mathcal{I}^-, \mathcal{I}^+$ and \mathcal{I} denote the sets of activations in the hidden layer where ℓ and u are both negative,
 275 both positive and span zero, respectively.

276 *Proof.* Given an example x , let $\tilde{x} = x + \delta$ be the perturbed input to the network. First, we explicit
 277 all the constraints for the linear program defined in (5):

$$\begin{aligned}
 & \min_{\hat{z}_3} [\hat{z}_3]_y - [\hat{z}_3]_{\bar{y}} = c^\top \hat{z}_3, \quad \text{s.t.} \\
 & \tilde{x} \in \mathcal{B}_\epsilon(x) \\
 & z_1 = \tilde{x} \\
 & \hat{z}_2 = W_1 z_1 + b_1 \\
 & \hat{z}_3 = W_2 z_2 + b_2 \\
 & [z_2]_j = 0, \quad \forall j \in \mathcal{I}^- \\
 & [z_2]_j = [\hat{z}_2]_j, \quad \forall j \in \mathcal{I}^+ \\
 & [z_2]_j \geq 0, \quad \forall j \in \mathcal{I} \\
 & [z_2]_j \geq [\hat{z}_2]_j, \quad \forall j \in \mathcal{I} \\
 & ((u_j - \ell_j) [z_2]_j - u_j [\hat{z}_2]_j) \leq -u_j \ell_j, \quad \forall j \in \mathcal{I}
 \end{aligned} \tag{16}$$

278 where \mathcal{I}^- , \mathcal{I}^+ and \mathcal{I} denote the sets of activations in the hidden layer where ℓ and u are both negative,
 279 both positive, or span zero respectively. In order to compute the dual of this problem, we associate
 280 the following Lagrangian variables with each of the constraints:

$$\begin{aligned}
 & \hat{z}_2 = W_1 z_1 + b_1 \Rightarrow \nu_2 \\
 & \hat{z}_3 = W_2 z_2 + b_2 \Rightarrow \nu_3 \\
 & z_1 = x + \delta \Rightarrow \psi \\
 & -[z_2]_j \leq 0 \Rightarrow \mu_j, \quad \forall j \in \mathcal{I} \\
 & [\hat{z}_2]_j - [z_2]_j \leq 0 \Rightarrow \tau_j, \quad \forall j \in \mathcal{I} \\
 & ((u_j - \ell_j) [z_2]_j - u_j [\hat{z}_2]_j) \leq -u_j \ell_j \Rightarrow \lambda_j, \quad \forall j \in \mathcal{I}
 \end{aligned} \tag{17}$$

281 note that we do not define explicit dual variables for $[z_2]_j = 0$ and $[z_2]_j = [\hat{z}_2]_j$ as we can easily
 282 eliminate them. We write the Lagrangian as follows:

$$\begin{aligned}
 \mathcal{L}(z, \hat{z}, \nu, \delta, \lambda, \tau, \mu, \psi) = & - (W_1^\top \nu_2 + \psi)^\top z_1 - \sum_{j \in \mathcal{I}} \left(\mu_j + \tau_j - \lambda_j (u_j - \ell_j) + [W_2^\top \nu_3]_j \right) [z_2]_j \\
 & + \sum_{j \in \mathcal{I}} (\tau_j - \lambda_j u_j + [\nu_2]_j) [\hat{z}_2]_j + (c + \nu_3)^\top \hat{z}_3 - \sum_{i=1}^2 \nu_{i+1}^\top b_i \\
 & + \sum_{j \in \mathcal{I}} \lambda_j u_j \ell_j + \psi^\top x + \psi^\top \delta + \sum_{j \in \mathcal{I}^-} [\hat{z}_2]_j [\nu_2]_j \\
 & + \sum_{j \in \mathcal{I}^+} [z_2]_j ([\nu_2]_j - [W_2^\top \nu_3]_j) \\
 & \text{s.t. } \tilde{x} \in \mathcal{B}_\epsilon(x)
 \end{aligned} \tag{18}$$

283 and we take the infimum w.r.t. z, \hat{z}, δ :

$$\begin{aligned}
 \inf_{z, \hat{z}, \delta} \mathcal{L}(z, \hat{z}, \nu, \delta, \lambda, \tau, \mu, \psi) = & - \inf_{z_2} \sum_{j \in \mathcal{I}} \left(\mu_j + \tau_j - \lambda_j (u_j - \ell_j) + [W_2^\top \nu_3]_j \right) [z_2]_j \\
 & + \inf_{\hat{z}_2} \sum_{j \in \mathcal{I}} (\tau_j - \lambda_j u_j + [\nu_2]_j) [\hat{z}_2]_j + \inf_{\hat{z}_3} (c + \nu_3)^\top \hat{z}_3 - \sum_{i=1}^2 \nu_{i+1}^\top b_i \\
 & + \sum_{j \in \mathcal{I}} \lambda_j u_j \ell_j + \psi^\top x + \inf_{\tilde{x} \in \mathcal{B}_\epsilon(x)} \psi^\top \tilde{x} - \inf_{z_1} (W_1^\top \nu_2 + \psi)^\top z_1 \\
 & + \inf_{\hat{z}_2} \sum_{j \in \mathcal{I}^-} [\hat{z}_2]_j [\nu_2]_j + \inf_{z_2} \sum_{j \in \mathcal{I}^+} [z_2]_j ([\nu_2]_j - [W_2^\top \nu_3]_j)
 \end{aligned} \tag{19}$$

284 Now, we compute the infimum for the $\psi^\top \delta$ term:

$$\inf_{\tilde{x} \in \mathcal{B}_\epsilon(x)} \psi^\top \tilde{x} = \inf_{\|\beta\|_1 \leq \epsilon} \psi_1 \cdot \beta = -\epsilon \cdot \|\psi_1\|_1 \tag{20}$$

285 and since for all the other terms the infimum of a linear function is $-\infty$, except in the special case
 286 when it is identically zero, the infimum of $\mathcal{L}(\cdot)$ becomes:

$$\inf_{z, \hat{z}, \delta} \mathcal{L}(\cdot) = \begin{cases} -\sum_{i=1}^2 \nu_{i+1}^\top b_i + \sum_{j \in \mathcal{I}} \lambda_j u_j \ell_j + \psi^\top x - \epsilon \|\psi_1\|_1 & \text{if conditions} \\ -\infty & \text{else} \end{cases} \quad (21)$$

287 where the conditions to satisfy are:

$$\begin{aligned} \nu_3 &= -c \\ W_1^\top \nu_2 &= -\psi \\ [\nu_2]_j &= 0, j \in \mathcal{I}_i^- \\ [\nu_2]_j &= [W_2^\top \nu_3]_j, j \in \mathcal{I}_i^+ \\ \left. \begin{aligned} (u_j - \ell_j) \lambda_j - \mu_j - \tau_j &= [W_2^\top \nu_3]_j \\ [\nu_2]_j &= u_j \lambda_j - \tau_j \end{aligned} \right\} j \in \mathcal{I} \\ \lambda, \tau, \mu &\geq 0 \end{aligned} \quad (22)$$

288 Thus, we can rewrite the dual problem as follows:

$$\begin{aligned} \max_{\nu, \psi, \lambda, \tau, \mu} & -\sum_{i=1}^2 \nu_{i+1}^\top b_i + \sum_{j \in \mathcal{I}} \lambda_j u_j \ell_j + \psi^\top x - \epsilon \|\psi_1\|_1 \\ \text{s.t.} & \quad \nu_3 = -c \\ & \quad W_1^\top \nu_2 = -\psi \\ & \quad [\nu_2]_j = 0, j \in \mathcal{I}_i^- \\ & \quad [\nu_2]_j = [W_2^\top \nu_3]_j, j \in \mathcal{I}_i^+ \\ & \quad \left. \begin{aligned} (u_j - \ell_j) \lambda_j - \mu_j - \tau_j &= [W_2^\top \nu_3]_j \\ [\nu_2]_j &= u_j \lambda_j - \tau_j \end{aligned} \right\} j \in \mathcal{I} \\ & \quad \lambda, \tau, \mu \geq 0 \end{aligned} \quad (23)$$

289 Note that the dual variable λ corresponds to the upper bounds in the convex ReLU relaxation, while μ
 290 and τ correspond to the lower bounds. By the complementarity property, we know that at the optimal
 291 solution, these variables will be zero if the ReLU constraint is non-tight, or non-zero if the ReLU
 292 constraint is tight. Since the upper and lower bounds cannot be tight simultaneously, either λ or
 293 $\mu + \tau$ must be zero. This means that at the optimal solution to the dual problem we can decompose
 294 $[W_2^\top \nu_3]_j$ into positive and negative parts since $(u_j - \ell_j)\lambda_j \geq 0$ and $\tau_j + \mu_j \geq 0$:

$$\begin{aligned} (u_j - \ell_j)\lambda_j &= [W_2^\top \nu_3]_j^+ \\ \tau_j + \mu_j &= [W_2^\top \nu_3]_j^- \end{aligned} \quad (24)$$

295 combining this with the constraint $[\nu_2]_j = u_j \lambda_j - \tau_j$ leads to

$$[\nu_2]_j = \frac{u_j}{u_j - \ell_j} [W_2^\top \nu_3]_j^+ - \alpha_j [W_2^\top \nu_3]_j^- \quad (25)$$

296 for $j \in \mathcal{I}$ and $0 \leq \alpha_j \leq 1$. Hence, we have that:

$$\lambda_j = \frac{u_j}{u_j - \ell_j} [\hat{\nu}_2]_j^+ \quad (26)$$

297 Now, we denote $\hat{\nu}_1 = -\psi$ to make our notation consistent, and putting all of this together the dual
 298 objective becomes:

$$\begin{aligned} -\sum_{i=1}^2 \nu_{i+1}^\top b_i + \sum_{j \in \mathcal{I}} \lambda_j u_j \ell_j + \psi^\top x - \epsilon \|\psi_1\|_1 &= -\sum_{i=1}^2 \nu_{i+1}^\top b_i + \sum_{j \in \mathcal{I}} \frac{u_j \ell_j}{u_j - \ell_j} [\hat{\nu}_2]_j^+ - \hat{\nu}_1^\top x - \epsilon \|\hat{\nu}_1\|_1 \\ &= -\sum_{i=1}^2 \nu_{i+1}^\top b_i + \sum_{j \in \mathcal{I}} \ell_j [\nu_2]_j^+ - \hat{\nu}_1^\top x - \epsilon \|\hat{\nu}_1\|_1 \end{aligned} \quad (27)$$

299 and the final dual problem:

$$\begin{aligned}
\max_{\nu, \hat{\nu}} \quad & -\sum_{i=1}^2 \nu_{i+1}^\top b_i + \sum_{j \in \mathcal{I}} \ell_j [\nu_2]_j^+ - \hat{\nu}_1^\top x - \epsilon \|\hat{\nu}_1\|_1 \\
\text{s.t.} \quad & \nu_3 = -c \\
& \hat{\nu}_2 = W_2^\top \nu_3 \\
& [\nu_2]_j = 0, \quad j \in \mathcal{I}^- \\
& [\nu_2]_j = [\hat{\nu}_2]_j, \quad j \in \mathcal{I}^+ \\
& [\nu_2]_j = \frac{u_j}{u_j - \ell_j} [\hat{\nu}_2]_j^+ - \alpha_j [\hat{\nu}_2]_j^-, \quad j \in \mathcal{I} \\
& \hat{\nu}_1 = W_1^\top \nu_2
\end{aligned} \tag{28}$$

300

□

301 B Approximations along the signal direction hurt generalisation

302 In this section, we further investigate our hypothesis that certified defences hurt generalisation when
303 adversarial perturbations are aligned with the signal direction. In particular, we study the linearly
304 separable distribution from the previous section and assume that the adversarial attacks concentrate
305 all of their perturbation budget along the signal direction. In Theorem B.1, we prove for a simple
306 neural network that, in high dimensions, certified defences (COAP) yield higher robust error than
307 empirical defences (AT) for large perturbation budgets. We then corroborate our theoretical results
308 with extensive experimental evidence on synthetic data.

309 **Data and threat models** We consider the linearly separable distribution described in Section 3.
310 As for the threat model, we consider signal-directed attacks that efficiently concentrate their attack
311 budget on the signal in the input. Since the signal direction corresponds to the first component of the
312 data, we define the set of allowed perturbations as:

$$\mathcal{B}_\epsilon(x) = \{z_1 = x + e_1 \beta \mid |\beta| \leq \epsilon\} \tag{29}$$

313 where e_1 is the standard basis vector of the first coordinate. Further, as the original formulation of
314 COAP only allows ℓ_p -adversaries, we provide an extension of COAP that covers our theoretical and
315 experimental setting in Appendix A.

316 **One gradient step training** We consider the hypothesis class to be the set of one-neuron shallow
317 neural networks $f_\theta : \mathbb{R}^d \rightarrow \mathbb{R}$, defined by:

$$f_\theta(x) = a \text{ReLU}(\theta^\top x) + b \tag{30}$$

318 where $x \in \mathbb{R}^d, \theta \in \mathbb{R}^d, a \in \mathbb{R}, b \in \mathbb{R}$ and the only trainable parameter is θ_1 . Note that as our
319 distribution is linearly separable, our hypothesis class includes the ground truth.

320 We study the early phase of neural network optimisation. Under structural assumptions on the data, it
321 has been proved that one gradient step with sufficiently large learning rate can drastically decrease the
322 training loss [3] and extract task-relevant features [9, 6]. A similar setting was also studied recently
323 in Ba et al. [1] for the MSE loss in the high-dimensional asymptotic limit. Here, we focus on the
324 classification setting with binary cross-entropy loss. Below we state our main theorem.

325 **Theorem B.1.** *Let $\bar{\theta}$ and $\tilde{\theta}$ be the network parameters after one step of gradient descent with respect*
326 *to AT and COAP objectives. Let,*

$$\frac{\|\theta_{2:d}\|_2}{\|\theta_1\|_2} > \sqrt{\frac{24\gamma^3}{\sigma^2}} \quad \text{and} \quad \frac{2}{3}\gamma < \epsilon < \gamma \tag{31}$$

327 where θ are the network parameters at initialization. Then, COAP yields higher robust risk than AT:

$$\mathbf{R}_\epsilon(\tilde{\theta}) > \mathbf{R}_\epsilon(\bar{\theta}) \tag{32}$$

328 Theorem B.1 relies on two main assumptions. The first is an assumption on the data dimensionality
329 and the initialisation of the network parameters θ . For instance, if the network parameters are
330 initialised sampling from a standard multivariate gaussian $\theta \sim \mathcal{N}(0, I_d)$, then we know that $\|\theta\|_2$

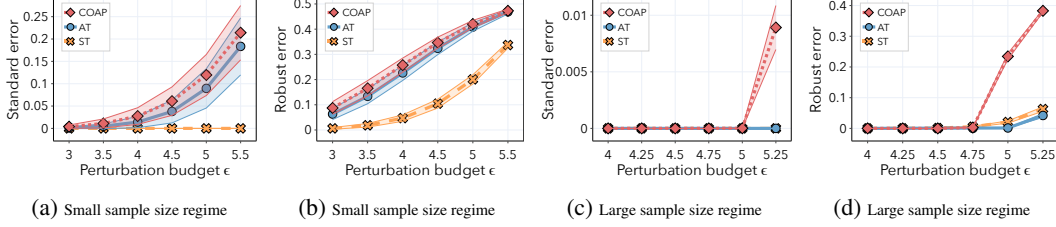


Figure 4: We report mean and standard deviation over 15 seeds. In Figure 4a and 4b we plot respectively the standard and robust errors in the small sample size ($n = 50$) regime for standard training (ST), adversarial training (AT) and convex outer adversarial polytope (COAP) as the perturbation budget ϵ increases. In Figure 4c and 4d we plot respectively the standard and robust errors in the large sample size ($n = 10000$) regime for standard training (ST), adversarial training (AT) and convex outer adversarial polytope (COAP) as the perturbation budget ϵ increases. See Appendix D.1 for complete experimental details.

331 concentrates around \sqrt{d} with high probability. Hence, the assumption is satisfied when the data
 332 dimensionality d is sufficiently high. Further, the second assumption requires that the perturbation
 333 budget ϵ is sufficiently close to the separation margin γ . This is consistent with the experimental
 334 evidence we presented so far, as the generalisation of certified defences significantly worsen for large
 335 perturbation budgets.

336 **Synthetic experiments** We corroborate our theory with experimental evidence using a one-hidden
 337 layer neural network with 100 neurons. In particular, we investigate the effect of perturbation budget ϵ
 338 on generalisation for three different models: standard training (ST), adversarial training (AT) [16, 11]
 339 and convex outer adversarial polytope (COAP) [25, 26]. In Figure 4, we plot robust and standard
 340 errors for both small and large sample size regimes as the perturbation budget ϵ increases. The
 341 generalisation gap in the small sample size regime between standard and adversarial training was
 342 already observed in Clarysse et al. [4] for linear classifiers. Here, we observe a further generalisation
 343 gap between AT and COAP in both small and large sample size regimes, which surprisingly worsens
 344 in the large sample regime.

345 C Theoretical results for signal-directed adversaries

346 We consider a similar generative distribution \mathbb{P} as in [4, 17, 23]: The label $y \in \{+1, -1\}$ is drawn
 347 with equal probability and the covariate vector is sampled for an $\gamma > 0$ as $x = [\gamma \operatorname{sgn}(y), \tilde{x}]$, with the
 348 random vector $\tilde{x} \in \mathbb{R}^{d-1}$ drawn from a standard normal distribution, $\tilde{x} \sim \mathcal{N}(0, \sigma^2 I_{d-1})$. We denote
 349 by $\mathcal{D} = \{(x_i, y_i)\}_{i=1}^n$ a dataset of size n i.i.d. drawn from \mathbb{P} . We consider the hypothesis class to be
 350 the set of one-neuron shallow neural networks $f_\theta : \mathbb{R}^d \rightarrow \mathbb{R}$:

$$f_\theta(x) = a \operatorname{ReLU}(\theta^\top x) + b \quad (33)$$

351 where $x \in \mathbb{R}^d$, $\theta \in \mathbb{R}^d$, $a \in \mathbb{R}$, $b \in \mathbb{R}$ and the only trainable parameter is θ_1 . Moreover, we assume
 352 w.l.o.g. that at initialisation $\theta_1 > 0$, and since a and b are not trainable parameters we must have $a > 0$
 353 and $b < 0$ to solve the problem. Note that as our distribution is linearly separable, our hypothesis
 354 class includes the ground truth. Further, we consider the binary cross-entropy loss function:

$$L(x, y) = y \log(x) + (1 - y) \log(1 - x) \quad (34)$$

355 C.1 Adversarial training gradients

356 Given a sample x with known label $y \in \{-1, 1\}$, we can find the point that minimizes this class by
 357 solving the following optimisation problem:

$$J_\epsilon = \min_{\delta} \operatorname{sgn}(y) f_\theta(x + \delta) \quad \text{subject to } x + \delta \in \mathcal{B}_\epsilon(x) \quad (35)$$

358 For our simplified network we have a closed form solution of this problem:

$$\begin{aligned}
J_\epsilon &= \min_{x+\delta \in \mathcal{B}_\epsilon(x)} \text{sgn}(y) (b + a \text{ReLU}(\theta^\top(x + \delta))) \\
&= \begin{cases} \text{sgn}(y) (b + a \max(0, \ell)) & \text{if } a \text{sgn}(y) > 0 \\ \text{sgn}(y) (b + a \max(0, u)) & \text{if } a \text{sgn}(y) < 0 \end{cases} \\
&= \begin{cases} \text{sgn}(y) (b + a \max(0, \ell)) & \text{if } \hat{\nu}_2 < 0 \\ \text{sgn}(y) (b + a \max(0, u)) & \text{if } \hat{\nu}_2 > 0 \end{cases}
\end{aligned} \tag{36}$$

359 where $\ell = \theta^\top x - \epsilon \theta_1$ and $u = \theta^\top x + \epsilon \theta_1$ are respectively lower and upper bounds on the pre-
360 activations. Thus, we can compute the gradients for adversarial training w.r.t the signal weight:

$$\frac{\partial}{\partial \theta_1} J_\epsilon = \begin{cases} \text{sgn}(y) a (x_1 - \epsilon \text{sgn}(\theta_1)) \mathbf{1}\{\ell > 0\} & \text{if } \hat{\nu}_2 < 0 \\ \text{sgn}(y) a (x_1 + \epsilon \text{sgn}(\theta_1)) \mathbf{1}\{u > 0\} & \text{if } \hat{\nu}_2 > 0 \end{cases} \tag{37}$$

361 and w.r.t. the non-signal weights ($k \geq 2$):

$$\frac{\partial}{\partial \theta_k} J_\epsilon = \begin{cases} \text{sgn}(y) a x_k \mathbf{1}\{\ell > 0\} & \text{if } \hat{\nu}_2 < 0 \\ \text{sgn}(y) a x_k \mathbf{1}\{u > 0\} & \text{if } \hat{\nu}_2 > 0 \end{cases} \tag{38}$$

362 Finally by the chain-rule we have:

$$\frac{\partial}{\partial \theta_k} L(\sigma(\text{sgn}(y) J_\epsilon), y) = \frac{\partial}{\partial J_\epsilon} L(\sigma(\text{sgn}(y) J_\epsilon), y) \cdot \frac{\partial}{\partial \theta_k} J_\epsilon \tag{39}$$

$$= \text{sgn}(y) [\sigma(\text{sgn}(y) J_\epsilon) - \mathbf{1}\{y = 1\}] \cdot \frac{\partial}{\partial \theta_k} J_\epsilon \tag{40}$$

$$= -\text{sgn}(y) \sigma(-J_\epsilon) \begin{cases} a x_k \mathbf{1}\{\ell > 0\} & \text{if } \hat{\nu}_2 < 0 \\ a x_k \mathbf{1}\{u > 0\} & \text{if } \hat{\nu}_2 > 0 \end{cases} \tag{41}$$

363 C.2 COAP gradients

364 We compute now the dual approximation \tilde{J}_ϵ to the optimisation problem (35), as defined in Theo-
365 rem A.1. In particular we are interested in the cases where $J_\epsilon \neq \tilde{J}_\epsilon$, that is when the certified and
366 adversarial training objectives differ. First, we consider the case when the neuron is always dead, i.e.,
367 $\ell < u < 0$. The dual variables are:

$$\begin{aligned}
\nu_3 &= -\text{sgn}(y) \\
\hat{\nu}_2 &= -a \text{sgn}(y) \\
\nu_2 &= 0 \\
\hat{\nu}_1 &= 0
\end{aligned} \tag{42}$$

368 Hence, there is no mismatch in this case:

$$\tilde{J}_\epsilon = \text{sgn}(y) b = J_\epsilon \tag{43}$$

369 where the last equality follows from (36).

370 Next, we consider the case when the neuron is always active, i.e., $0 < \ell < u$. The dual variables are:

$$\begin{aligned}
\nu_3 &= -\text{sgn}(y) \\
\hat{\nu}_2 &= -a \text{sgn}(y) \\
\nu_2 &= -a \text{sgn}(y) \\
\hat{\nu}_1 &= -a \text{sgn}(y) \cdot \theta
\end{aligned} \tag{44}$$

371 and the dual objective becomes:

$$\tilde{J}_\epsilon = -\nu_3^\top b - \hat{\nu}_1^\top x - \epsilon \|\hat{\nu}_1\|_1 \tag{45}$$

$$= \text{sgn}(y) (b + a(\theta^\top x)) - \epsilon \|a \text{sgn}(y) \theta\| \tag{46}$$

$$= \begin{cases} \text{sgn}(y) (b + a\ell) & \text{if } a \text{sgn}(y) > 0 \\ \text{sgn}(y) (b + au) & \text{if } a \text{sgn}(y) < 0 \end{cases} \tag{47}$$

$$= J_\epsilon \tag{48}$$

372 where the last equality follows from the fact that $0 < \ell < u$.
 373 Finally, we consider the case when the neuron is in the activation set \mathcal{I} , i.e., $\ell < 0 < u$. The dual
 374 variables are:

$$\begin{aligned}\nu_3 &= -\operatorname{sgn}(y) \\ \hat{\nu}_2 &= -a \operatorname{sgn}(y) \\ \nu_2 &= -a \operatorname{sgn}(y) \frac{u}{2\epsilon \|\theta_1\|_1} \\ \hat{\nu}_1 &= -a \operatorname{sgn}(y) \frac{u}{2\epsilon \|\theta_1\|_1} \cdot \theta\end{aligned}\tag{49}$$

375 Here we have two cases, when $\hat{\nu}_2 > 0$ we can rewrite the dual objective as:

$$\tilde{J}_\epsilon = \operatorname{sgn}(y) (b + au) = J_\epsilon\tag{50}$$

376 hence the dual approximation is tight. When $\nu_2 < 0$ we can rewrite the dual objective as:

$$\tilde{J}_\epsilon = \operatorname{sgn}(y) \left(b + \frac{au\ell}{2\epsilon \|\theta_1\|_1} \right) \neq J_\epsilon\tag{51}$$

377 It follows that the only case when certified training differs from adversarial training is when $\nu_2 < 0$
 378 and the neuron belongs to the activation set \mathcal{I} . We compute the partial derivative w.r.t. the signal
 379 weight θ_1 in this case, by the chain rule we have:

$$\frac{\partial}{\partial \theta_1} L \left(\sigma \left(\operatorname{sgn}(y) \cdot \tilde{J}_\epsilon \right), y \right)\tag{52}$$

$$= \frac{\partial}{\partial \tilde{J}_\epsilon} L \left(\sigma \left(\operatorname{sgn}(y) \cdot \tilde{J}_\epsilon \right), y \right) \cdot \frac{\partial}{\partial \theta_1} \tilde{J}_\epsilon\tag{53}$$

$$= \operatorname{sgn}(y) \left[\sigma \left(\operatorname{sgn}(y) \cdot \tilde{J}_\epsilon \right) - \mathbf{1}\{y = 1\} \right] \cdot \frac{\partial}{\partial \theta_1} \tilde{J}_\epsilon\tag{54}$$

$$= -\frac{a \operatorname{sgn}(y) \sigma \left(-\tilde{J}_\epsilon \right)}{2\epsilon} \left(\frac{\ell}{\|\theta_1\|_1} (x_1 + \epsilon \operatorname{sgn}(\theta_1)) + u \frac{x_1 \|\theta_1\|_1 - \theta^\top x \operatorname{sgn}(\theta_1)}{\theta_1^2} \right)\tag{55}$$

380 and finally we compute the partial derivative w.r.t. the non-signal weight $\theta_k (k \geq 2)$:

$$\frac{\partial}{\partial \theta_k} L \left(\sigma \left(\operatorname{sgn}(y) \cdot \tilde{J}_\epsilon \right), y \right)\tag{56}$$

$$= \frac{\partial}{\partial \tilde{J}_\epsilon} L \left(\sigma \left(\operatorname{sgn}(y) \cdot \tilde{J}_\epsilon \right), y \right) \cdot \frac{\partial}{\partial \theta_k} \tilde{J}_\epsilon\tag{57}$$

$$= \operatorname{sgn}(y) \left[\sigma \left(\operatorname{sgn}(y) \cdot \tilde{J}_\epsilon \right) - \mathbf{1}\{y = 1\} \right] \cdot \frac{\partial}{\partial \theta_k} \tilde{J}_\epsilon\tag{58}$$

$$= -\frac{ax_k \operatorname{sgn}(y) \sigma \left(-\tilde{J}_\epsilon \right) \theta^\top x}{\epsilon \|\theta_1\|_1}\tag{59}$$

381 C.3 Auxiliary lemmas

382 **Lemma C.1.** *Let f_θ be the neural network defined in Equation (33). We define the robust risk \mathbf{R}_ϵ of*
 383 *f_θ as follows:*

$$\mathbf{R}_\epsilon(\theta) := \mathbb{P}_{(x,y)} [\exists z \in \mathcal{B}_\epsilon(x) : y \neq \operatorname{sgn}(f_\theta(z))]\tag{60}$$

384 *Then, $\mathbf{R}_\epsilon(\theta)$ is monotonically decreasing in $\|\theta_1\|_2$.*

Proof.

$$\mathbf{R}_\epsilon(\theta) := \mathbb{P}_{(x,y)} [\exists z \in \mathcal{B}_\epsilon(x) : y \neq \text{sgn}(f_\theta(z))] \quad (61)$$

$$= \frac{1}{2} (\mathbb{P}_x [\theta^\top x < \|b\|_1 \mid x_1 = \gamma - \epsilon] + \mathbb{P}_x [\theta^\top x > \|b\|_1 \mid x_1 = \epsilon - \gamma]) \quad (62)$$

$$= \frac{1}{2} \left(\mathbb{P}_x \left[\sum_{i=2}^d x_i \theta_i < -\theta_1(\gamma - \epsilon) + \|b\|_1 \right] + \mathbb{P}_x \left[\sum_{i=2}^d x_i \theta_i > \theta_1(\gamma - \epsilon) + \|b\|_1 \right] \right) \quad (63)$$

$$= \frac{1}{2} \left(\Phi \left(-\frac{(\gamma - \epsilon) \|\theta_1\|_2}{\sigma \|\theta_{2:d}\|_2} + \frac{\|b\|_1}{\sigma \|\theta_{2:d}\|_2} \right) + \Phi \left(-\frac{(\gamma - \epsilon) \|\theta_1\|_2}{\sigma \|\theta_{2:d}\|_2} - \frac{\|b\|_1}{\sigma \|\theta_{2:d}\|_2} \right) \right) \quad (64)$$

385 hence $\mathbf{R}_\epsilon(\theta)$ is monotonically decreasing in $\|\theta_1\|_2$ and the statement follows. \square

386 **Lemma C.2.** *Let $f : \mathbb{R} \rightarrow \mathbb{R}$ be the function defined by $f(x) = \exp(x)$. When $x \leq 0$ and n is even*
387 *we have:*

$$f(x) \leq 1 + x + \frac{x^2}{2!} + \cdots + \frac{x^n}{n!} \quad (65)$$

388 *Proof.* Let $g : (-\infty, 0] \rightarrow \mathbb{R}$ be the function defined by

$$g(x) = 1 + x + \frac{x^2}{2!} + \cdots + \frac{x^n}{n!} - \exp(x) \quad (66)$$

389 Since $g(x) \rightarrow \infty$ as $x \rightarrow -\infty$, g must attain an absolute minimum somewhere on the interval
390 $(-\infty, 0]$. Now, differentiating we have:

391 • If f has an absolute minimum at 0, then for all x , $f(x) \geq f(0) = 1 - \exp(0) = 0$, so we
392 are done.

• If f has an absolute minimum at y for some $y < 0$, then $f'(y) = 0$. But differentiating,

$$f'(y) = 1 + y + \frac{y^2}{2!} + \cdots + \frac{y^{n-1}}{(n-1)!} - \exp(y) = f(y) - \frac{y^n}{n!}.$$

Therefore, for any x ,

$$f(x) \geq f(y) = \frac{y^n}{n!} + f'(y) = \frac{y^n}{n!} > 0,$$

393 since n is even.

394 \square

395 **Lemma C.3.** *Let $f : \mathbb{R}^2 \rightarrow \mathbb{R}$ be the function defined by $f(x, y) = \Phi(y) - \Phi(x)$. When $x < y < 0$*
396 *we have:*

$$\phi(0) \left(y - x + \frac{x^3}{6} \right) \leq \Phi(y) - \Phi(x) \quad (67)$$

397 *Proof.* First, we want to prove that $\frac{2x}{\sqrt{\pi}}$ is a lower bound for the error function $\text{erf}(x)$ when $x \leq 0$.

398 That is, we want to show that $f(x) \geq 0$ where $f : (-\infty, 0] \rightarrow \mathbb{R}$ is the function defined by:

$$f(x) = \text{erf}(x) - \frac{2x}{\sqrt{\pi}} \quad (68)$$

399 Since f is continuous and $f(x) \rightarrow \infty$ as $x \rightarrow -\infty$, f must attain an absolute minimum on the
400 interval $(-\infty, 0]$. Now, differentiating we have:

$$f'(x) = \frac{2}{\sqrt{\pi}} \exp(-x^2) - \frac{2}{\sqrt{\pi}} \quad (69)$$

401 hence f attains an absolute minimum at 0 and we have $f(x) \geq f(0) = 0$.

402 Next, we show that $\frac{2}{\sqrt{\pi}}(x - x^3/3)$ is an upper bound for $\text{erf}(x)$ when $x \leq 0$. Let $g : (-\infty, 0] \rightarrow \mathbb{R}$
403 the function defined by:

$$g(x) = \frac{2}{\sqrt{\pi}}(x - x^3/3) - \text{erf}(x) \quad (70)$$

404 Similarly, since g is continuous and $g(x) \rightarrow \infty$ as $x \rightarrow -\infty$, g must attain an absolute minimum
 405 on the interval $(-\infty, 0]$. Now, differentiating we have:

$$g'(x) = \frac{2}{\sqrt{\pi}}(1 - x^2 - \exp(-x^2)) \quad (71)$$

406 hence g attains an absolute minimum at 0 and we have $g(x) \geq g(0) = 0$.
 407 Now, since $a < b < 0$ we can use the erf bounds derived above:

$$\Phi(b) - \Phi(a) = \frac{1}{2} \left(\operatorname{erf}(b/\sqrt{2}) - \operatorname{erf}(a/\sqrt{2}) \right) \quad (72)$$

$$\geq \frac{1}{\sqrt{\pi}} \left(\frac{b}{\sqrt{2}} - \frac{a}{\sqrt{2}} + \frac{a^3}{6\sqrt{2}} \right) \quad (73)$$

$$= \phi(0) \left(b - a + \frac{a^3}{6} \right) \quad (74)$$

408 which concludes the proof. \square

409 **Lemma C.4.** Suppose $f : \mathbb{R} \rightarrow \mathbb{R}$ is defined as follows:

$$f(r) = \gamma^2 - \epsilon^2 - 2\sigma^2 r^2 - \sigma r \frac{(\gamma - 3\epsilon)\phi(\beta) - (\gamma + \epsilon)\phi(\alpha)}{\Phi(\beta) - \Phi(\alpha)} \quad (75)$$

410 where $\alpha := -\frac{\gamma+\epsilon}{r\sigma}$, $\beta := -\frac{\gamma-\epsilon}{r\sigma}$, Φ and ϕ are respectively the standard normal cdf and pdf. Assume
 411 that:

$$\frac{5 + 2\sqrt{3}}{13} \gamma < \epsilon < \gamma \quad (76)$$

412 Then, we have:

$$f(r) < 0, \quad \forall r > \sqrt{\frac{24\gamma^3}{\sigma^2}} \quad (77)$$

413 *Proof.* We begin by providing a lower bound on the difference of gaussian cdfs. Applying Lemma
 414 C.3 with $x = \alpha$ and $y = \beta$ we have:

$$\Phi(\beta) - \Phi(\alpha) \geq \left(\frac{2\epsilon}{r\sigma} - \frac{(\gamma + \epsilon)^3}{6\sigma^3 r^3} \right) \phi(0), \quad \alpha < \beta < 0 \quad (78)$$

415 Next, we can upper-bound f :

$$f(r) \leq \gamma^2 - \epsilon^2 - 2\sigma^2 r^2 - \sigma r \frac{(\gamma - 3\epsilon)\phi(\beta) - (\gamma + \epsilon)\phi(\alpha)}{\left(\frac{2\epsilon}{r\sigma} - \frac{(\gamma + \epsilon)^3}{6\sigma^3 r^3} \right) \phi(0)} \quad (79)$$

$$\leq \gamma^2 - \epsilon^2 - 2\sigma^2 r^2 - \sigma^2 r^2 \frac{(\gamma - 3\epsilon)\phi(0) - (\gamma + \epsilon)\phi(\alpha)}{\left(2\epsilon - \frac{(\gamma + \epsilon)^3}{6r^2\sigma^2} \right) \phi(0)} \quad (80)$$

$$= \gamma^2 - \epsilon^2 - 2\sigma^2 r^2 - \sigma^2 r^2 \frac{(\gamma - 3\epsilon) - (\gamma + \epsilon)\exp(-\alpha^2/2)}{2\epsilon - \frac{(\gamma + \epsilon)^3}{6\sigma^2 r^2}} \quad (81)$$

416 Now, we use the upper-bound for the exponential function from Lemma C.2 with $n = 2$:

$$\exp(x) \leq 1 + x - x^2/2, \quad \forall x \leq 0 \quad (82)$$

417 and substituting it back into our upper-bound for f we get:

$$f(r) \leq \gamma^2 - \epsilon^2 - 2\sigma^2 r^2 - \sigma^2 r^2 \frac{(\gamma - 3\epsilon) - (\gamma + \epsilon)\left(1 - \frac{(\gamma + \epsilon)^2}{2r^2\sigma^2} + \frac{(\gamma + \epsilon)^4}{8r^4\sigma^4}\right)}{2\epsilon - \frac{(\gamma + \epsilon)^3}{6r^2\sigma^2}} \quad (83)$$

418 which can be further simplified:

$$f(r) \leq \gamma^2 - \epsilon^2 - 2\sigma^2 r^2 - \sigma^2 r^2 \frac{(\gamma - 3\epsilon) - (\gamma + \epsilon) \left(1 - \frac{(\gamma + \epsilon)^2}{2r^2 \sigma^2} + \frac{(\gamma + \epsilon)^4}{8r^4 \sigma^4}\right)}{2\epsilon - \frac{(\gamma + \epsilon)^3}{6r^2 \sigma^2}} \quad (84)$$

$$= \frac{(\gamma - 7\epsilon)(\gamma + \epsilon)^4 + 4r^2 \sigma^2 (\gamma + \epsilon)(\gamma^2 - 10\gamma\epsilon + 13\epsilon^2)}{4(\gamma + \epsilon)^3 - 48r^2 \sigma^2 \epsilon} \quad (85)$$

$$= u(r) \quad (86)$$

419 and we have that for $\epsilon > \frac{5+2\sqrt{3}}{13}\gamma$ and $r > \sqrt{\max\left(\frac{(7\epsilon - \gamma)(\gamma + \epsilon)^4}{4\sigma^2(\gamma^2 - 10\gamma\epsilon + 13\epsilon^2)}, \frac{(\gamma + \epsilon)^3}{12\sigma^2 \epsilon}\right)}$ the upper bound is
 420 negative, i.e. $u(r) < 0$. Finally, for the sake of clarity we can further simplify the condition on r :

$$r > \sqrt{\frac{24\gamma^3}{\sigma^2}} > \sqrt{\max\left(\frac{(7\epsilon - \gamma)(\gamma + \epsilon)^4}{4\sigma^2(\gamma^2 - 10\gamma\epsilon + 13\epsilon^2)}, \frac{(\gamma + \epsilon)^3}{12\sigma^2 \epsilon}\right)} \quad (87)$$

421 which concludes the proof. \square

422 **Lemma C.5.** Let f_θ the network defined in Equation (33), \tilde{J}_ϵ be the COAP training objective, $\sigma(\cdot)$
 423 the sigmoid function and $\mathcal{I}^* = \{(x, y) : \ell < 0 \wedge u > 0 \wedge y = 1\}$. Assume that:

$$\frac{\|\theta_{2:d}\|_2}{\|\theta_1\|_2} > \sqrt{\frac{24\gamma^3}{\sigma^2}} \quad \text{and} \quad \frac{5 + 2\sqrt{3}}{13}\gamma < \epsilon < \gamma \quad (88)$$

424 Then, we have:

$$\mathbb{E}_{(x,y)} \left[\nabla_{\theta_1} L \left(\sigma \left(\text{sgn}(y) \tilde{J}_\epsilon \right), y \mid (x, y) \in \mathcal{I}^* \right) \right] > 0 \quad (89)$$

425 *Proof.* Our strategy will be to lower-bound the expectation in Equation (89) with some strictly
 426 positive quantity. We define $Z = \sum_{i=2}^d \theta_i x_i$ and plug-in the gradient computed in Appendix C.2:

$$\mathbb{E}_{(x,y)} \left[\nabla_{\theta_1} L \left(\text{sgn}(y) \sigma \left(\tilde{J}_\epsilon \right), y \mid (x, y) \in \mathcal{I}^* \right) \right] \quad (90)$$

$$= \mathbb{E}_{(x,y)} \left[\frac{a\sigma(-\tilde{J}_\epsilon)}{2\epsilon} \left(-\frac{\ell}{\theta_1}(\gamma + \epsilon) + u \frac{\sum_{i=2}^d x_i \theta_i}{\theta_1^2} \right) \mid (x, y) \in \mathcal{I}^* \right] \quad (91)$$

$$= \frac{a}{2\theta_1 \epsilon} \mathbb{E}_{(x,y)} \left[\sigma(-\tilde{J}_\epsilon) \left(-\ell(\gamma + \epsilon) + u \frac{Z}{\theta_1} \right) \mid (x, y) \in \mathcal{I}^* \right] \quad (92)$$

$$= \frac{a}{2\theta_1 \epsilon} \mathbb{E}_{(x,y)} \left[\sigma(-\tilde{J}_\epsilon) u \frac{Z}{\theta_1} - \sigma(-\tilde{J}_\epsilon) \ell(\gamma + \epsilon) \mid (x, y) \in \mathcal{I}^* \right] \quad (93)$$

427 Now, we observe that Z is always negative on the set \mathcal{I}^* :

$$(x, y) \in \mathcal{I}^* \implies -\theta_1(\gamma + \epsilon) < \sum_{i=2}^d \theta_i x_i < -\theta_1(\gamma - \epsilon) < 0 \quad (94)$$

428 since we need to satisfy the constraint $\ell < 0 < u$. Further, from Equation (51) we have:

$$(x, y) \in \mathcal{I}^* \implies \sigma(-\tilde{J}_\epsilon) \geq \frac{1}{2} \quad (95)$$

429 Combining these two observations we can lower-bound the expectation:

$$\mathbb{E}_{(x,y)} \left[\nabla_{\theta_1} L \left(\text{sgn}(y) \sigma \left(\tilde{J}_\epsilon \right), y \mid (x, y) \in \mathcal{I}^* \right) \right] \quad (96)$$

$$= \frac{a}{2\theta_1 \epsilon} \mathbb{E}_{(x,y)} \left[\sigma(-\tilde{J}_\epsilon) u \frac{Z}{\theta_1} - \sigma(-\tilde{J}_\epsilon) \ell(\gamma + \epsilon) \mid (x, y) \in \mathcal{I}^* \right] \quad (97)$$

$$\geq \frac{a}{2\theta_1 \epsilon} \mathbb{E}_{(x,y)} \left[u \frac{Z}{\theta_1} - \frac{\gamma + \epsilon}{2} \ell \mid (x, y) \in \mathcal{I}^* \right] \quad (98)$$

430 Hence for our purpose it is enough to show that this lower-bound is strictly positive:

$$\mathbb{E}_{(x,y)} \left[u \frac{Z}{\theta_1} - \frac{\gamma + \epsilon}{2} \ell \mid (x, y) \in \mathcal{I}^* \right] > 0 \quad (99)$$

431 we can further expand this expression:

$$\mathbb{E}_{(x,y)} \left[u \frac{Z}{\theta_1} - \frac{\gamma + \epsilon}{2} \ell \mid (x, y) \in \mathcal{I}^* \right] \quad (100)$$

$$= -(\gamma^2 - \epsilon^2)\theta_1^2 + (\gamma + \epsilon)\theta_1 \mathbb{E}[Z \mid (x, y) \in \mathcal{I}^*] + 2\mathbb{E}[Z^2 \mid (x, y) \in \mathcal{I}^*] \quad (101)$$

432 Note that $Z \mid (x, y) \in \mathcal{I}^*$ is a truncated normal with $\alpha = -\frac{\theta_1(\gamma+\epsilon)}{\sigma\|\theta_{2:d}\|_2}$, $\beta = -\frac{\theta_1(\gamma-\epsilon)}{\sigma\|\theta_{2:d}\|_2}$. Hence, we can
433 plug the expectations in and obtain the following:

$$-(\gamma^2 - \epsilon^2)\theta_1^2 + \theta_1(\gamma + \epsilon)\mathbb{E}[Z \mid (x, y) \in \mathcal{I}^*] + 2\mathbb{E}[Z^2 \mid (x, y) \in \mathcal{I}^*] \quad (102)$$

$$= -(\gamma^2 - \epsilon^2)\theta_1^2 + 2\sigma^2 \|\theta_{2:d}\|_2^2 + \sigma \|\theta_{2:d}\|_2 \theta_1 \frac{(\gamma - 3\epsilon)\phi(\beta) - (\gamma + \epsilon)\phi(\alpha)}{\Phi(\beta) - \Phi(\alpha)} \quad (103)$$

$$\propto -(\gamma^2 - \epsilon^2) + 2\sigma^2 r^2 + \sigma r \frac{(\gamma - 3\epsilon)\phi(\beta) - (\gamma + \epsilon)\phi(\alpha)}{\Phi(\beta) - \Phi(\alpha)} \quad (104)$$

$$= -f(r) \quad (105)$$

434 where we define $r = \frac{\|\theta_{2:d}\|_2}{\|\theta_1\|_2}$. Now, under our assumption, from Lemma C.4 we have:

$$f(r) < 0, \forall r > \sqrt{\frac{24\gamma^3}{\sigma^2}} \quad (106)$$

435 which concludes the proof. \square

436 C.4 Proof of Theorem B.1

437 **Theorem B.1.** Let $\bar{\theta}$ and $\tilde{\theta}$ be the network parameters after one step of gradient descent with respect
438 to AT and COAP objectives. Let,

$$\frac{\|\theta_{2:d}\|_2}{\|\theta_1\|_2} > \sqrt{\frac{24\gamma^3}{\sigma^2}} \quad \text{and} \quad \frac{2}{3}\gamma < \epsilon < \gamma \quad (31)$$

439 where θ are the network parameters at initialization. Then, COAP yields higher robust risk than AT:

$$\mathbf{R}_\epsilon(\tilde{\theta}) > \mathbf{R}_\epsilon(\bar{\theta}) \quad (32)$$

440 *Proof.* Let J_ϵ be the adversarial training inner maximisation as defined in Equation (35). Then, AT
441 solves the following optimisation problem:

$$\min_{\theta} \mathbb{E}_{(x,y)} [L(\sigma(\text{sgn}(y)J_\epsilon), y)] \quad (107)$$

442 Similarly, let \tilde{J}_ϵ be the COAP dual approximation to the inner maximization described in Appendix
443 C.2. Then, COAP solves the following optimisation problem:

$$\min_{\theta} \mathbb{E}_{(x,y)} \left[L\left(\sigma\left(\text{sgn}(y)\tilde{J}_\epsilon\right), y\right) \right] \quad (108)$$

444 In what follows, $\bar{\theta}^{(t)}$ refers to the parameter trained with adversarial training at iteration t and $\tilde{\theta}^{(t)}$ to
445 the COAP counterpart. After one step of gradient descent, we have:

$$\left\| \bar{\theta}_{2:d}^{(1)} \right\|_2 = \left\| \tilde{\theta}_{2:d}^{(1)} \right\|_2 \quad (109)$$

446 since we only train the signal component. Further, from Lemma C.1 we have that adversarial training
447 yields smaller robust risk than certified if the following to holds:

$$\left\| \bar{\theta}_1^{(1)} \right\|_2 > \left\| \tilde{\theta}_1^{(1)} \right\|_2 \quad (110)$$

448 which, after one step of gradient descent, is equivalent to:

$$\mathbb{E}_{(x,y)} [\nabla_{\bar{\theta}_1} L(\sigma(\text{sgn}(y)J_\epsilon), y)] < \mathbb{E}_{(x,y)} [\nabla_{\bar{\theta}_1} L(\sigma(\text{sgn}(y)\tilde{J}_\epsilon), y)] \quad (111)$$

449 In Appendix C.2 and C.1 we compute gradients for both objectives. In particular, we have that the
450 gradients of adversarial and certified training differ only on the set \mathcal{I}^* :

$$(x, y) \notin \mathcal{I}^* \implies \nabla_{\bar{\theta}_1} L(\sigma(\text{sgn}(y)J_\epsilon), y) = \nabla_{\bar{\theta}_1} L(\sigma(\text{sgn}(y)\tilde{J}_\epsilon), y) < 0 \quad (112)$$

451 and

$$(x, y) \in \mathcal{I}^* \implies 0 = \nabla_{\bar{\theta}_1} L(\sigma(\text{sgn}(y)J_\epsilon), y) \neq \nabla_{\bar{\theta}_1} L(\sigma(\text{sgn}(y)\tilde{J}_\epsilon), y) \quad (113)$$

452 Hence for our purpose it is enough to show that:

$$\mathbb{E}_{(x,y)} [\nabla_{\bar{\theta}_1} L(\sigma(\text{sgn}(y)\tilde{J}_\epsilon), y) \mid (x, y) \in \mathcal{I}^*] > 0 \quad (114)$$

453 which is a direct consequence of Lemma C.5. Thus we have that:

$$\|\bar{\theta}_1\|_2 > \|\tilde{\theta}_1\|_2 \quad \text{and} \quad \|\bar{\theta}_{2:d}\|_2 = \|\tilde{\theta}_{2:d}\|_2 \quad (115)$$

454 and from Lemma C.1 follows:

$$\mathbf{R}_\epsilon(\tilde{\theta}) > \mathbf{R}_\epsilon(\bar{\theta}) \quad (116)$$

455 which concludes the proof. \square

456 D Experimental details

457 D.1 Synthetic experiments with signal-directed adversaries

458 Below we provide detailed experimental details to reproduce Figure 4. For all the experiments, we use
459 the one hidden layer architecture defined in Equation (2) with 100 neurons. We use PyTorch SGD op-
460 timiser and train all networks for 100 epochs. We sweep over the learning rate $\eta \in \{0.1, 0.01, 0.001\}$
461 and for each perturbation budget, we choose the one that interpolates the training set and minimises
462 robust error on the test set. We perform all the attacks to evaluate robust risk at test-time using exact
463 line search; this is computationally tractable since the attacks are directed along one dimension.

464 For the linearly separable distribution we set $d = 1000$, $n_{\text{test}} = 10^5$, $\gamma = 6$.

465 **Standard training.** We train the network to minimise the cross-entropy loss.

466 **Adversarial training** [16, 11]. We train the network to minimise the robust binary cross-entropy loss.
467 At each epoch, we compute an exact adversarial example using line search and update the weights
468 using a gradient with respect to this example.

469 **Certified training** [25, 26]. At each epoch, we compute upper and lower bounds u and ℓ as described
470 in Proposition A.2. We then train the network to minimize the upper-bound on robust error derived in
471 Theorem A.1.

472 D.2 Synthetic experiments with ℓ_2 adversaries

473 Below we provide detailed experimental details to reproduce Figure 3.

474 For the spheres dataset, we consider a data distribution similar to Gilmer et al. [10] that consists of
475 two concentric spheres in d dimensions: we generate a random $x \in \mathbb{R}^d$ where $\|x\|_2$ is either γ_{\min} or
476 γ_{\max} , with equal probability assigned to each norm. We associate with each x a label y such that
477 $y = 0$ if $\|x\|_2 = \gamma_{\min}$ and $y = 1$ if $\|x\|_2 = \gamma_{\max}$. We can sample uniformly from this distribution by
478 sampling $z \sim \mathcal{N}(0, I_d)$ and then setting $x = \frac{z}{\|z\|_2} \gamma_{\min}$ or $x = \frac{z}{\|z\|_2} \gamma_{\max}$.

479 For the linearly separable distribution we set $d = 1000$, $n = 50$, $n_{\text{test}} = 10^5$, $\gamma = 6$. For the
480 concentric spheres distribution we set $d = 100$, $n = 50$, $n_{\text{test}} = 10^5$, $\gamma_{\min} = 1$ and $\gamma_{\max} = 12$.

481 For all the experiments, we use the MLP architecture with $W = 100$ neurons in each hidden layer
482 and ReLU (\cdot) activation functions. We use PyTorch SGD optimiser with a momentum of 0.95 and

483 train the network for 150 epochs. We sweep over the learning rate $\eta \in \{0.1, 0.01, 0.001\}$ and for
484 each perturbation budget, we choose the one that minimises robust error on the test set among the
485 classifiers that interpolate the training set. We perform the attacks to evaluate robust risk at test-time
486 using Auto-PGD [5] with 100 iterations and 5 random restarts. We use both the cross-entropy and
487 difference of logits loss to prevent gradient masking. For all attacks we use the implementation
488 provided in AutoAttack [5] with some adjustments to allow for non-image inputs.

489 **Standard training.** We train the network to minimise the cross-entropy loss.

490 **Adversarial training** [16, 11]. We train the network to minimise the robust cross-entropy loss. At
491 each epoch, we search for adversarial examples using Auto-PGD with a budget of 10 steps and 1
492 random restart. Then, we update the weights using a gradient with respect to this example.

493 **Certified training** [25, 26]. We consider the tightest convex relaxation, i.e. the convex outer
494 adversarial polytope derived in Wong and Kolter [25]. We train the network to minimise their
495 upper-bound on the robust error. Our implementation is based on the code released by the authors.

496 **D.3 Image experiments**

497 Below we provide experimental details to reproduce Figures 2.

498 For CIFAR-10, we train the residual network (ResNet) with the same structure used in Wong et al.
499 [26]. For MNIST, we train the large convolutional neural network (CNN) architecture (see Table 1)
500 introduced in Wong et al. [26], with four convolutional layer and two fully connected layers of 512
501 units.

502 For MNIST we use full 28×28 images without any augmentations and normalization. For CIFAR-10
503 we use random horizontal flips and random crops as data augmentation, and normalize images
504 according to per-channel statistics.

505 For all ℓ_p -adversaries considered, we evaluate the robust error using the most expensive version of
506 AutoAttack (AA+) [5], which includes the following attacks:

- 507 • untargeted APGD-CE (5 restarts)
- 508 • untargeted APGD-DLR (5 restarts)
- 509 • untargeted APGD-DLR (5 restarts)
- 510 • Square Attack (5000 queries)
- 511 • targeted APGD-DLR (9 target classes)
- 512 • targeted FAB (9 target classes)

513 **AT training details** For MNIST, we train 100 epochs using Adam optimiser [13] with a learning
514 rate of 0.001, momentum of 0.9 and a batch size of 128; we reduce the learning rate by a factor 0.1 at
515 epochs 40 and 80. For CIFAR-10 and ResNet, we train 150 epochs using SGD with a learning rate of
516 0.05 and a batch size of 128; we reduce the learning rate by a factor 0.1 at epochs 80 and 120. For
517 the inner optimisation, adversarial examples are generated with 10 iterations of Auto-PGD [5].

518 **COAP training details** We follow the settings proposed by the authors and report them here. For
519 MNIST, we use the Adam optimiser with a learning rate of 0.001 and a batch size of 50. We schedule
520 ϵ starting from 0.01 to the desired value over the first 20 epochs, after which we decay the learning
521 rate by a factor of 0.5 every 10 epochs for a total of 60 epochs. For CIFAR-10, we use the SGD
522 optimiser with a learning rate of 0.05 and a batch size of 50. We schedule ϵ starting from 0.001 to the
523 desired value over the first 20 epochs, after which we decay the learning rate by a factor of 0.5 every
524 10 epochs for a total of 60 epochs. For all experiments, we use random projection of 50 dimensions.

525 **CROWN-IBP training details** For MNIST, we train 200 epochs with a batch size of 256. We use
526 Adam optimizer and set learning rate to 5×10^{-4} . We warm up with 10 epochs of regular training,
527 and gradually ramp up ϵ_{train} from 0 to ϵ in 50 epochs. We reduce the learning rate by a factor 0.1 at
528 epoch 130 and 190. For CIFAR-10, we train 2000 epochs with a batch size of 256, and a learning rate
529 of 5×10^{-4} . We warm up for 100 epochs, and ramp-up ϵ for 800 epochs. Learning rate is reduced by
530 a factor 0.1 at epoch 1400 and 1700. For Tiny ImageNet, we train 600 epochs with batch size 128.

531 The first 100 epochs are clean training, then we gradually increase ϵ_{train} with a schedule length of 400.
 532 For all datasets, an hyper-parameter β to balance LiRPA bounds and IBP bounds for the output layer
 533 is gradually decreased from 1 to 0 (1 for only using LiRPA bounds and 0 for only using IBP bounds),
 534 with the same schedule of ϵ . For all experiments, we use the implementation provided in the auto
 535 LiRPA library [28].

CNN-SMALL	CNN-LARGE
CONV 16 $4 \times 4 + 2$	CONV 32 $3 \times 3 + 1$
CONV 32 $4 \times 4 + 1$	CONV 32 $4 \times 4 + 2$
FC 100	CONV 64 $3 \times 3 + 1$
	CONV 64 $4 \times 4 + 2$
	FC 512
	FC 512

Table 1: Model architectures. All layers are followed by $\text{ReLU}(\cdot)$ activations. The last fully connected layer is omitted. "CONV $k w \times h + s$ " corresponds to a 2D convolutional layer with k filters of size $w \times h$ using a stride of s in both dimensions. "FC n " corresponds to a fully connected layer with n outputs.